Electrical Power and Energy Systems 159 (2024) 110047

Contents lists available at ScienceDirect

International Journal of Electrical Power and Energy Systems

journal homepage: www.elsevier.com/locate/ijepes

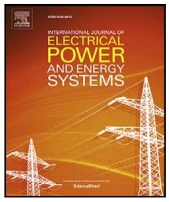

Renewable-dominated mobility-as-a-service framework for resilience delivery in hydrogen-accommodated microgrids

Jinshun Su [a], Ruotan Zhang [a], Payman Dehghanian [a,*], Mohammad Heidari Kapourchali [b], Sungyun Choi [c], Zhaohao Ding [d]

[a] Department of Electrical and Computer Engineering, The George Washington University, 800 22nd Street NW, Washington, DC, 20052, USA
[b] Department of Electrical Engineering, University of Alaska Anchorage, 2900 Spirit Dr, Anchorage, AK, 99508, USA
[c] School of Electrical Engineering, Korea University, 145 Anam-ro, Seongbuk-gu, Seoul, 02841, South Korea
[d] School of Electrical and Electronic Engineering, North China Electric Power University, 2 Beinong Rd, Beijing, 102206, China

ARTICLE INFO

Keywords:
Mobile wind turbine (MWT)
Hydrogen storage system (HSS)
Service restoration
Decarbonization
High-impact low-probability (HILP)

ABSTRACT

The growing utilization of wind energy resources has been evidenced to have had substantial positive impacts on mitigating climate change consequences. Unlike stationary wind turbines, mobile wind turbines (MWTs) can travel along the local transportation system (TS) via a truck, supplying power to microgrids (MGs). This spatiotemporal flexibility can provide significant benefits, including enhancing system resilience in the aftermath of high-impact low-probability (HILP) events and contributing to energy system decarbonization. In this paper, we propose a two-stage stochastic optimization model for the service restoration problem by coordinating the routing and scheduling of MWTs with hydrogen storage systems (HSSs) in MGs. The first-stage problem focuses on optimizing the deployment of MWTs based on the shortest-path information obtained through Dijkstra's algorithm. The second-stage problem aims to minimize the expected power outage costs while accounting for wind energy uncertainties estimated through a Monte Carlo simulation approach. Case studies on an integrated transportation and energy network – a central Alabama interstate TS and four IEEE 33-node test power systems – demonstrate the effectiveness of the proposed restoration scheme in boosting MGs resilience and reducing carbon emissions.

1. Introduction

Climate change is driving global warming, resulting in a growing prevalence of high-impact low-probability (HILP) events on a global scale. Such HILP incidents – e.g., hurricanes, wildfires, winter storms – have led to excessive equipment damages, prolonged electricity outages, significant economic losses, and disruptions in our modern society [1]. Fig. 1 demonstrates the increasing frequency of extreme natural disasters in the United States in 2021 and 2022 [2], most of which resulted in extensive electricity outages. Power outages triggered by climate change have inflicted substantial economic losses and posed significant threats to human life, underscoring the critical need for improving power grid resilience [3]. Global warming changes atmospheric circulation and ocean currents, which could alter the location, timing, track, and intensity of hurricanes [4]. For instance, Hurricane Maria in Puerto Rico in 2017 caused disruptions in 31 major power-generating units in 20 facilities and left the entire island without electricity [5]. The impact of Hurricane Sandy in 2012 was severe, with approximately 10% of customers in New York and New Jersey experiencing a 10-day power outage, resulting in economic losses estimated nearly $26 billion and tragically causing 50 deaths due to the prolonged lack of electricity [6]. Moreover, climate change due to carbon emissions leads to higher temperatures, amplifying the occurrence of wildfires in forested regions characterized by high fuel aridity [7]. For example, the Wine Country of Northern California was hit by a series of wildfires that began in October 2017, resulting in insured damages of over $9.4 billion and the loss of 44 lives [8]. In 2020, the United States experienced the second-largest area impacted by wildfires in a single year since 1960, with a total of 58,950 wildfire incidents burning 10.1 million acres [9]. Additionally, climate change can intensify and alter the severity of winter storms by destabilizing weather patterns, increasing moisture content in the atmosphere, and disrupting the polar jet stream [10]. In February 2021, an extreme winter storm caused a massive electricity generation failure in Texas, which led to more than 4.5 million households without electricity at its peak for several days and approximately $130 billion in economic losses [11]. The

* Corresponding author.
E-mail address: payman@gwu.edu (P. Dehghanian).

https://doi.org/10.1016/j.ijepes.2024.110047
Received 13 June 2023; Received in revised form 22 January 2024; Accepted 14 May 2024

Nomenclature

Sets

$\mathbf{M}$	Set of mobile wind turbines (MWTs).
$\mathbf{K}$	Set of nodes in the transportation system (TS).
$\mathbf{T}$	Set of time periods in the decision-making horizon.
$\boldsymbol{\Phi}$	Set of microgrids (MGs).
$\mathbf{I}_\phi$	Set of nodes in the MG ϕ.
$\mathbf{I}_\phi^c \subset \mathbf{I}_\phi$	Set of candidate nodes in the MG ϕ.
$\mathbf{K}^d \subset \mathbf{K}$	Set of nodes hosting depots in the TS.
$\mathbf{S}$	Set of scenarios.
$\mathbf{H}$	Set of hydrogen storage systems (HSSs).
$\mathbf{L}_\phi$	Set of power lines in the MG ϕ.

Parameters and Constants

δ_m	Transportation cost coefficient of MWT m.
C_k	Maximum number of MWTs allowed to be connected to TS node k.
$T^r_{k\hat{k}}$	Travel time from TS nodes k to $\hat{k}$.
$\Lambda_{k\phi i}$	Binary parameter equal to 1 if TS node k is mapped to candidate node i of MG ϕ, 0 otherwise.
π_s	Probability of scenario s.
$a_{\phi i}$	Interrupted energy assessment rate for node i of MG ϕ.
$b_{\phi t}$	Price of undelivered energy from electric utility of MG ϕ at time t.
$P^D_{\phi it}, Q^D_{\phi it}$	Real/Reactive power demand in node i of MG ϕ at time t.
P^G_ϕ, Q^G_ϕ	Real/Reactive power capacity of substation at MG ϕ.
$\underline{\theta}_{\phi i}, \overline{\theta}_{\phi i}$	Lower/Upper bounds of power factor angle at node i of MG ϕ.
$P^F_{\phi l}, Q^F_{\phi l}$	Real/Reactive power flow capacity of line l of MG ϕ.
V^{ref}_ϕ	Reference squared voltage magnitude at MG ϕ.
U	Big M number.
$\lambda_{\phi lt}$	Binary parameter equal to 1 if the power line l of MG ϕ is energized at time t, 0 otherwise.
$R_{\phi l}, X_{\phi l}$	Resistance/Reactance of power line l of MG ϕ.
$\underline{V}^{sq}_{\phi i}, \overline{V}^{sq}_{\phi i}$	Minimum/Maximum squared voltage magnitude at node i of MG ϕ.
$\rho_{h\phi i}$	Binary parameter equal to 1 if HSS h is located at node i of MG ϕ, 0 otherwise.
$E^{ini}_h, \underline{E}_h, \overline{E}_h$	Initial/Minimum/Maximum hydrogen storage level of HSS h.
$\eta^{p2h}_h, \eta^{h2p}_h$	Power-to-hydrogen (P2H)/Hydrogen-to-power (H2P) efficiency of HSS h.
$\sigma^{p2h}_h, \sigma^{h2p}_h$	P2H/H2P conversion factor of HSS h.
$\overline{P}^{p2h}_h, \overline{P}^{h2p}_h$	Maximum capacity of consumed/generated power of HSS h in P2H/H2P mode.
W^{Cap}_m	Wind power capacity of MWT m.
$\xi^w_{\phi ts}$	Random parameter of predicted wind energy at MG ϕ at time t in scenario s.

Variables

α_{mkt}	Binary variable equal to 1 if MWT m is connected to TS node k at time t, 0 otherwise.
$\beta_{m\phi it}$	Binary variable equal to 1 if MWT m is connected to node i of MG ϕ at time t, 0 otherwise.
γ_{mt}	Binary variable equal to 1 if MWT m is traveling at time t, 0 otherwise.
$\mu^{p2h}_{hts}, \mu^{h2p}_{hts}$	Binary variable equal to 1 if HSS h is in P2H/H2P mode at time t in scenario s, 0 otherwise.
$p^{out}_{\phi its}, q^{out}_{\phi its}$	Real/Reactive power outage in node i of MG ϕ at time t in scenario s.
$\Psi_{m\phi its}$	Power injection from individual MWT m to node i of MG ϕ at time t in scenario s.
$p^w_{\phi its}$	Total power injection from all possible MWTs to node i of MG ϕ at time t in scenario s.
$v^{sq}_{\phi its}$	Squared voltage magnitude at node i of MG ϕ at time t in scenario s.
$p^{p2h}_{hts}, p^{h2p}_{hts}$	Consumed/Generated power of HSS h in P2H/H2P mode at time t in scenario s.
E_{hts}	Hydrogen storage level of HSS h at time t in scenario s.
$p^g_{\phi its}, q^g_{\phi its}$	Total real/reactive power injection to node i of MG ϕ at time t in scenario s.
$p^f_{\phi lts}, q^f_{\phi lts}$	Real/Reactive power flow in line l of MG ϕ at time t in scenario s.
p^{net}_{hts}	The net power output of HSS h at time t in scenario s.

substantial economic losses and profound societal disruptions stemming from these events have underscored the critical importance and urgent need to address the consequences of climate change while fortifying power grid resilience against such extremes.

It is important to recognize that the heavy reliance of the conventional power system on fossil fuels, with high levels of carbon emissions, is exacerbating climate change and contributing to the escalation of increasingly severe weather conditions [12]. Consequently, the development of sustainable energy systems becomes imperative to mitigate the impacts of climate change and the resulting HILP incidents. In response to these environmental concerns, renewable and clean energy resources have been widely adopted and integrated into modern power systems [13]. The rapid deployment of distributed energy resources, including solar photovoltaics, wind turbines, and hydrogen energy, can significantly reduce carbon emissions and enhance the resilience of the power grid in the face of extreme events [14].

In the past decade, extensive research has been conducted on the utilization of wind power for system restoration. Notably, in [15], the authors demonstrate that incorporating wind power into the energy dispatch model enables fast restoration procedures. Taking into account the vulnerability of power grid elements, [16] presents an effective restoration strategy that incorporates wind energy participation, aiming to achieve an elevated level of grid resilience in the face of widespread emergencies. Additionally, the study [17] explores the coordination of wind farms and pumped-storage hydro units to enhance power system resilience through a stochastic security-constraint unit commitment

(a) 2021 (b) 2022

Fig. 1. Extreme natural disasters in the U.S. in 2021 and 2022 [2].

framework. The study [18] develops an adaptive robust optimization model to facilitate a faster and more reliable self-healing process by coordinating wind farms and pumped-storage hydro units. The study [19] proposes an optimization method for loop-network reconfiguration during the black-start process, considering the integration of large-scale wind power. Furthermore, the study [20] presents a rolling optimization model for power system restoration that incorporates a hybrid wind-storage system and accounts for the uncertainty of wind power using a chance-constrained approach. The study [21] introduces a model predictive control-based voltage regulation strategy, enabling wind farms to offer the black-start capability.

In addition to leveraging locally-sourced energy for power restoration, the utilization of mobile power sources (MPSs) holds significant promise for enabling spatiotemporal flexibility exchange within MGs. This approach has garnered growing interest due to its potential to enhance system resilience and improve overall system efficiency. For instance, a joint post-disaster restoration scheme applying MPSs and distributed generators tackling the transportation system (TS) constraints is proposed in [22]. The study in [23] introduced a rolling integrated service restoration strategy for MPSs scheduling and routing, which captures the uncertainty in the status of the roads and electric branches in coupled transportation-power networks. A lexicographic multi-objective model is applied in [24] to ensure a maximum resiliency plan during emergencies by the optimal scheduling of MPSs with a rolling horizon operation model. Considering the integration of the MPSs and repair crews dispatch, the study in [25] proposes a co-optimization approach formulated as a mixed-integer second-order cone programming model for distribution system resilience. The study in [1] presents automated decision-making solutions for boosting the resilience and operational endurance of mission-critical systems and services during disasters, coordinating the utilization of MPSs with schedules of repair crews, taking into account constraints in both power and transportation networks. The study in [26] proposes a co-optimization model including MPSs, repair crews, and soft-open-point networked MGs for the power distribution system resilience improvement. The study in [27] proposes a two-stage restoration scheme for distribution system restoration harnessing the full potential of MPSs dispatch jointly with the dynamic distribution system reconfiguration under a suite of seismic force scenarios. A three-stage approach coordinating MPSs dispatch and forced cut-off of wind power is proposed in [28] to enhance the survivability and restoration of distribution systems. The study in [29] develops a novel restoration mechanism in distribution systems for deployment of MPSs, capturing the uncertainty in renewable energy resources with joint probabilistic constraints. The study in [30] considers decision-dependent uncertainty in the availability of MPSs due to travel and waiting times to offer a more realistic estimation of the MPSs' contributions to distribution system resilience enhancement. Focusing on the strategic deployment of MPSs, the research presented in [31] introduces a risk-averse model that is designed to formulate a public safety power-shutoff plan that effectively balances the risks of wildfires with the incidence of power outages.

State-of-art literature exploring the utilization of MPSs for service restoration primarily focuses on coal-consuming MPSs such as mobile emergency generators [22,24–26,30,31]. However, it is crucial to harness the untapped potential of cleaner and renewable resources in MPSs utilization. The introduction of mobile wind turbines (MWTs), which are transportable small-scale units, offers a viable solution to reduce carbon emissions while actively participating in the system restoration process. Furthermore, existing studies [1,23] that have investigated the routing and scheduling of MPSs, accounting for the interdependence of the MG and the TS, have predominantly focused on urban areas. To the best of our knowledge, the existing literature lacks analytical solutions for MWT utilization and dispatch that account for the coupling between the MG and the TS in rural localities. To fill in this knowledge gap, this paper explores, for the first time, a two-stage stochastic optimization model for the service restoration problem via MWTs routing and scheduling in rural regions. In particular, we propose a novel two-stage stochastic optimization model that integrates the dispatch of MWTs with the operation of hydrogen storage systems (HSSs) in MGs. The model takes into consideration the uncertainties associated with wind energy forecasts by incorporating a Monte Carlo simulation approach. The proposed model presents an effective integration of multiple MGs and a TS into a unified framework, enabling the spatiotemporal utilization of wind energy in rural areas. To enhance the efficiency and cost-effectiveness of MWTs' dispatch decisions, the model leverages the shortest-path algorithm. Through extensive numerical experiments, the proposed model demonstrates the significant benefits and efficacy in enhancing the resilience of MGs, as well as promisingly achieving key decarbonization objectives. Our findings also offer valuable managerial insights on how to strike a balance between minimizing power outage costs and reducing carbon emissions. This information can aid decision-makers in making informed choices to optimize the sustainability and resilience of MGs in the face of HILP incidents.

The rest of the paper is organized as follows. Section 2 presents an overview of MWT technologies and hydrogen-accommodated MGs. Section 3 describes the proposed service restoration framework. Section 4 presents the proposed two-stage stochastic optimization formulation. Case studies are analyzed in Section 5 and research findings are summarized in Section 6.

2. Background

2.1. Mobile wind turbines (MWTs)

MWTs are small-scale wind turbines that are designed to be easily transportable. Typically, these turbines are mounted on trailers or other mobile platforms to facilitate their transport to the desired location for power generation [32]. Fig. 2 illustrates a typical MWT [33], where the turbine can be stored in a pickup trailer, allowing for convenient transportation and setup.

MWTs are commonly used for off-grid power generation or to power remote locations. Due to their clean and renewable energy generation

Fig. 2. A typical mobile wind turbine setup [33].

capacity, MWTs are gaining popularity in various settings, including disaster relief efforts, powering remote communities, temporary power for events or construction sites, and other applications [32]. The versatility of MWTs is a significant advantage, making them suitable for use in different environments, including rural regions with low wind speeds and urban areas with high wind speeds [34]. The study [35] incorporates joint utilization of MWTs and electric thermal storage units into the MG energy portfolio, which can shift the load profile and prevent costs associated with peak demand. With spatiotemporal flexibility, MWTs serve as an exceptional choice for providing emergency power to damaged power systems in the face of extreme weather conditions. They can improve the resilience of rural power systems during emergencies and reduce carbon emissions, thus supporting environmentally-friendly energy generation to mitigate the adverse effects of climate change.

2.2. Hydrogen-accommodated microgrids

Hydrogen-accommodated MGs are small-scale power systems that incorporate hydrogen technologies to enable efficient storage and use of renewable energy resources. The need to address climate change has made it imperative to operate the power system in a low-carbon manner. Hydrogen systems are increasingly being recognized as a crucial means of storing renewable energy due to their carbon-neutral nature and high-capacity storage capabilities that support long-term energy regulation [36]. Fig. 3 illustrates the interconnection between the operations of a power system and the HSS [37]. The HSS comprises units of water electrolyzer, hydrogen storage, and fuel cell. This setup allows excess power to be harnessed and stored in hydrogen storage tanks. Later, when there is a demand for power, the stored hydrogen can be converted into electricity using fuel cells.

2.3. Integration of MWTs in hydrogen-accommodated microgrids

In this research, we explore the integration of MWTs with hydrogen-accommodated MGs to improve the resilience of the system following disturbances. Essentially, this involves considering the combined operation of MWTs and HSSs in the context of service restoration. Fig. 4 provides a visual representation of the role played by MWTs and HSSs in the MGs' restoration efforts under varying conditions of wind power availability and load requirements. In *Region I*, where there is abundant wind power and high electricity demand, MWTs deliver a substantial amount of power to the MGs. Concurrently, HSSs supply the additional power needed to meet this high demand. During *Region II*, characterized by ample wind power but a lower load demand, MWTs again provide significant power to the MGs. The surplus power generated in this scenario is directed for storage in the HSSs. *Region III* represents a scenario with limited wind power availability and low demand. Here, the power contribution of MWTs to the MGs is relatively low, and HSSs inject the necessary power to fulfill the demand. Lastly, in *Region IV*,

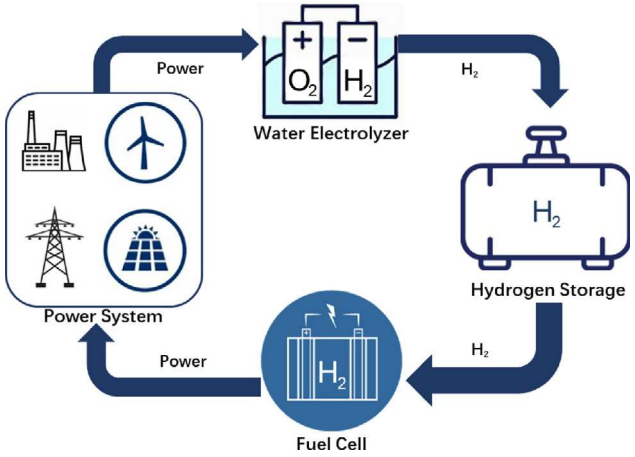

Fig. 3. On the role of hydrogen systems in a renewable-integrated power grid.

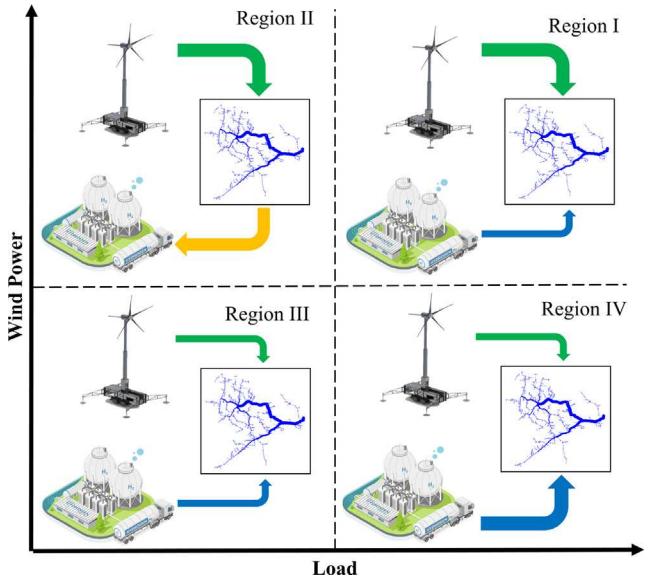

Fig. 4. Joint operation of MWTs and HSSs in MGs under different wind availability and load requirement conditions.

where wind power is scarce but the load requirement is high, MWTs can only supply a small portion of the needed power to the MGs. In this case, HSSs play a crucial role by injecting a considerably larger amount of power, typically more than the other regions, to meet the high demand.

3. Problem description

3.1. General framework

The proposed optimization framework, as illustrated in Fig. 5, is designed to address the challenges associated with the coordination of MWTs and HSSs in MGs for power restoration. **Step 1** involves the collection of information. Following an HILP event at time t_{k-1}, when initial conditions on the power line failure in MGs and the status of the transportation system (TS) roads are gathered at time t_k. This information, essential for decision-making in service restoration, is considered deterministic. A shortest-path algorithm is employed to determine the travel times for each TS road. However, the predicted wind power for upcoming periods remains uncertain. To address this, we use Monte Carlo simulation for generating wind power prediction

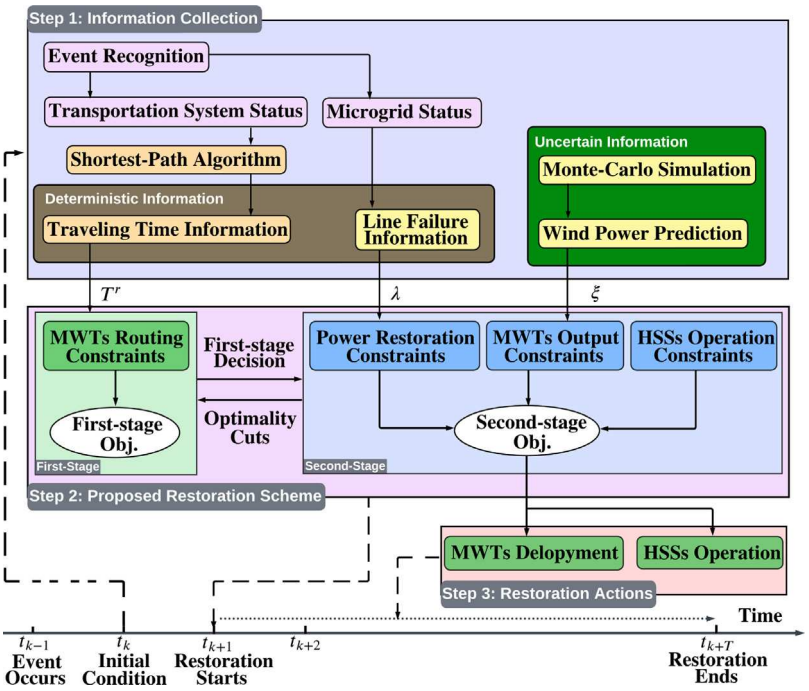

Fig. 5. Overarching framework of the proposed two-stage restoration scheme.

scenarios, aiding in optimal decision-making. With the information from **Step 1**, a two-stage stochastic optimization model is applied in **Step 2**, guiding system operators in the restoration of MGs. The first stage focuses on optimizing MWT deployment based on the current TS status. As wind power, crucial for MWTs, is variable and uncertain, the second stage aims to minimize the expected costs of power outages, taking into account the wind power uncertainty. In **Step 3**, the assignment for MWTs and HSSs operation is determined. Accordingly, system operators can execute the optimal restoration decisions from time t_{k+1} to t_{k+T}.

In this study, it is considered that MWTs can provide power to rural areas affected by outages, facilitating the quicker restoration and thereby reducing the costs associated with power outages. The power output of an MWT depends not only on its capacity but also on the amount of wind power available in the surrounding environment. According to Fig. 5, the information on the predicted wind power is characterized as the source of uncertainty. When the realizations of predicted wind power in different scenarios are revealed in the second stage, the cost of power outage in each scenario could be determined due to the deployment of MWTs in the first stage. Therefore, the optimal decisions for routing and scheduling of MWTs under uncertainty under a predicted wind power availability can be efficiently obtained via a two-stage stochastic optimization problem.

3.2. Shortest-path algorithm

The shortest-path algorithm, a fundamental concept in graph theory and network optimization, aims to identify the shortest route between two nodes in a given graph. This algorithm has been widely employed in various applications, such as transportation, communication, and logistics [38]. In the context of MWTs deployment, the use of the shortest-path algorithm is crucial for maximizing efficiency and cost-effectiveness. The primary rationale for employing this algorithm is to optimize the MWTs' travel time between different locations, which is critical considering the dynamic and time-sensitive nature of wind energy production. By minimizing the overall distance and travel duration, MWTs can be effectively and rapidly deployed in areas where wind conditions are optimal. Consequently, this approach ensures maximum energy output while reducing fuel consumption and carbon emissions associated with transportation. In this paper, the travel time of MWTs is obtained by Dijkstra's algorithm, which solves the single-source shortest-path problem for a graph with non-negative edge weights [39].

3.3. Wind forecast scenario generation

Modeling wind speed is critical to accurately predicting wind energy production. In this regard, the Weibull distribution is often used due to its ability to model uncorrelated wind speeds [40]. By estimating the parameters of the Weibull distribution, one can effectively predict wind speed distributions, including the mean and standard deviation [41]. In this study, we utilize the Monte Carlo simulation to generate wind forecast scenarios based on the Weibull distribution. Monte Carlo simulation produces a large number of scenarios for the stochastic parameters, which are based on forecasted values and the typical distribution of each parameter [42]. In order to reduce the computational complexity and the number of scenarios to a tractable size, we employ the Backward Scenario Reduction algorithm [43]. This algorithm uses the Kantorovich distance to remove scenarios and assign their probability to the closest remaining scenario. By generating a tractable number of realistic wind forecast scenarios, we can facilitate the development of an effective optimization model for power restoration in MGs.

4. Model formulation

To strengthen the resilience of hydrogen-based MGs in the context of renewable-dominated mobility-as-a-service following extreme weather events, a two-stage stochastic optimization model has been developed that addresses uncertainties associated with wind energy. The first-stage problem focuses on optimizing the routing and scheduling of MWTs coordinated with the operation of multiple MGs and the TS. In the second-stage problem, the objective is to minimize the expected power outage costs while accounting for wind energy uncertainties. The proposed model is formulated as a mixed-integer linear programming (MILP) problem. To ease the notations, we define

index sets $\boldsymbol{\Omega} = \{(m,k,\phi,i,t) : m \in \mathbf{M}, k \in \mathbf{K}, \phi \in \boldsymbol{\Phi}, i \in \mathbf{I}_\phi, t \in \mathbf{T}\}$, $\hat{\boldsymbol{\Omega}} = \{(m,\phi,i,l,t,s) : m \in \mathbf{M}, \phi \in \boldsymbol{\Phi}, i \in \mathbf{I}_\phi, l \in \mathbf{L}_\phi, t \in \mathbf{T}, s \in \mathbf{S}\}$, and $\tilde{\boldsymbol{\Omega}} = \{(\phi,t,s) : \phi \in \boldsymbol{\Phi}, t \in \mathbf{T}, s \in \mathbf{S}\}$.

4.1. First-stage problem: MWTs dispatch decisions

The first-stage problem concentrates on making decisions on the assignment of MWTs based on the shortest-path information in the TS (see Section 3.2). The objective function in the first-stage problem is expressed as follows:

$$\min_{\mathbf{x}\in\mathcal{X}} \sum_{m\in\mathbf{M}}\sum_{t\in\mathbf{T}} \delta_m \gamma_{mt} + f(\mathbf{x},\boldsymbol{\xi}) \tag{1}$$

$$\mathbf{x} = \{\alpha_{mkt}, \beta_{m\phi it}, \gamma_{mt} | (m,k,\phi,i,t) \in \boldsymbol{\Omega}\} \subseteq \{0,1\} \tag{2}$$

where $\mathbf{x}$ represents the vector of the binary variables in the first-stage problem. The first term denotes the transportation cost of MWTs during the restoration phase, which is attributed to the trips they make. The second term $f(\mathbf{x},\boldsymbol{\xi})$ represents the objective function in the second-stage problem depending on the first-stage decisions $\mathbf{x}$ and the vector of random variables $\boldsymbol{\xi}$. The first-stage decision variables are subject to the following constraints:

$$\mathcal{X} =$$

$$\alpha_{mk(t+\tau)} \le 1 - \alpha_{m\hat{k}t}, \qquad m \in \mathbf{M}, k, \hat{k} \in \mathbf{K}, \tau \le T^r_{k\hat{k}}, t \le |\mathbf{T}| - \tau \tag{3}$$

$$\alpha_{mk1} = 1, \qquad m \in \mathbf{M}, k \in \mathbf{K}^d \tag{4}$$

$$\sum_{m\in\mathbf{M}} \alpha_{mkt} \le C_k, \qquad k \in \mathbf{K}, t \in \mathbf{T} \tag{5}$$

$$\sum_{k\in\mathbf{K}} \alpha_{mkt} \le 1, \qquad m \in \mathbf{M}, t \in \mathbf{T} \tag{6}$$

$$\alpha_{mkt} \ge \Lambda_{k\phi i}\beta_{m\phi it}, \qquad k \in \mathbf{K}, m \in \mathbf{M}, i \in \mathbf{I}^c_\phi, \phi \in \boldsymbol{\Phi}, t \in \mathbf{T} \tag{7}$$

$$\beta_{m\phi it} = 0, \qquad m \in \mathbf{M}, i \in \mathbf{I}_\phi \setminus \mathbf{I}^c_\phi, \phi \in \boldsymbol{\Phi}, t \in \mathbf{T} \tag{8}$$

$$\gamma_{mt} = 1 - \sum_{k\in\mathbf{K}} \alpha_{mkt}, \qquad m \in \mathbf{M}, t \in \mathbf{T} \tag{9}$$

The routing of MWTs is defined by constraint (3). For example, if MWT m is at TS node k at time $t = 1$ (i.e., $\alpha_{mk1} = 1$) and needs 2 time periods to travel from node k to $\hat{k}$ (i.e., $T^r_{k\hat{k}} = 2$)—meaning that MWT m is on its way from node k to $\hat{k}$ at time periods $t = 2$ and $t = 3$, then MWT m arrive at candidate node $\hat{k}$ at $t = 4$ (i.e., $\alpha_{m\hat{k}4} = 1$), which implies $\alpha_{m\hat{k}1} = 0$, $\alpha_{m\hat{k}2} = 0$, and $\alpha_{m\hat{k}3} = 0$. Constraint (4) specifies the initial location of the MWT, while constraint (5) ensures that the total number of MWTs located at TS node k at any time period does not exceed the maximum number of vehicles that node k can host. Each MWT m can stay in at most one node at any time period as enforced by constraint (6). In an MG, candidate nodes are nodes equipped with specific electrical facilities that allow MWTs to be connected to the MG. There exists a correspondence between the MG candidate nodes and the TS nodes, hereafter called *coupling points/nodes* [1]. Constraint (7) ensures that the MG candidate node i can be served by MWT m only if it reaches the coupling node k of the TS at time t. Constraint (8) stipulates that an MWT cannot be dispatched to a non-candidate node in the MG. It should be noted that an MWT can only be in one of the two states in each time period: either connected to the MG or traveling on the TS, reflected in constraint (9).

4.2. Second-stage problem: Service restoration in MGs

In the second-stage problem, the focus is on restoring MGs following an event. The objective is to minimize the expected costs of power outages, taking into account the decisions made in the first-stage problem regarding the dispatch of MWTs and the uncertainties associated with wind energy. The objective function in the second-stage problem is formulated below:

$$f(\mathbf{x},\boldsymbol{\xi}) = \min_{\boldsymbol{\nu},\mathbf{y},\mathbf{z}\in\Xi(\mathbf{x},\boldsymbol{\xi})} \sum_{s\in\mathbf{S}} \pi_s \sum_{\phi\in\boldsymbol{\Phi}}\sum_{i\in\mathbf{I}_\phi}\sum_{t\in\mathbf{T}} (a_{\phi i} + b_{\phi t}) p^{out}_{\phi its} \tag{10}$$

$$\boldsymbol{\nu} = \{\mu^{p2h}_{hts}, \mu^{h2p}_{hts} | h \in \mathbf{H}, t \in \mathbf{T}, s \in \mathbf{S}\} \subseteq \{0,1\} \tag{11}$$

$$\mathbf{y} = \{p^{out}_{\phi its}, q^{out}_{\phi its}, \psi_{m\phi its}, p^{w}_{\phi its}, v^{sq}_{\phi its} | (m,\phi,i,l,t,s) \in \hat{\boldsymbol{\Omega}}\} \cup \{p^{p2h}_{hts}, p^{h2p}_{hts}, E_{hts} | h \in \mathbf{H}, t \in \mathbf{T}, s \in \mathbf{S}\} \subseteq \mathbb{R}_+ \tag{12}$$

$$\mathbf{z} = \{p^{g}_{\phi its}, q^{g}_{\phi its}, p^{f}_{\phi lts}, q^{f}_{\phi lts} | (m,\phi,i,l,t,s) \in \hat{\boldsymbol{\Omega}}\} \cup \{p^{net}_{hts} | h \in \mathbf{H}, t \in \mathbf{T}, s \in \mathbf{S}\} \subseteq \mathbb{R} \tag{13}$$

where $\boldsymbol{\nu}$, $\mathbf{y}$, and $\mathbf{z}$ represent the vectors of binary variables, nonnegative continuous variables, and continuous variables in the second-stage problem, respectively. The objective function (10) aims to minimize the expected costs of power outages including the interruption cost imposed to customers (i.e., $a_{\phi i} p^{out}_{\phi its}$) and the revenue-loss imposed to the electric utility (i.e., $b_{\phi t} p^{out}_{\phi its}$). The second-stage decision variables are subject to the following constraints:

$$\Xi(\mathbf{x},\boldsymbol{\xi}) =$$

$$\sum_{\substack{l\in\mathbf{L}_\phi;\\ \Theta(l)=i}} p^f_{\phi lts} - \sum_{\substack{l\in\mathbf{L}_\phi;\\ \Gamma(l)=i}} p^f_{\phi lts} = p^g_{\phi its} - (P^D_{\phi it} - p^{out}_{\phi its}), \qquad i \in \mathbf{I}_\phi, (\phi,t,s) \in \tilde{\boldsymbol{\Omega}} \tag{14}$$

$$\sum_{\substack{l\in\mathbf{L}_\phi;\\ \Theta(l)=i}} q^f_{\phi lts} - \sum_{\substack{l\in\mathbf{L}_\phi;\\ \Gamma(l)=i}} q^f_{\phi lts} = q^g_{\phi its} - (Q^D_{\phi it} - q^{out}_{\phi its}), \qquad i \in \mathbf{I}_\phi, (\phi,t,s) \in \tilde{\boldsymbol{\Omega}} \tag{15}$$

$$0 \le p^{out}_{\phi its} \le P^D_{\phi it}, \qquad i \in \mathbf{I}_\phi, (\phi,t,s) \in \tilde{\boldsymbol{\Omega}} \tag{16}$$

$$0 \le q^{out}_{\phi its} \le Q^D_{\phi it}, \qquad i \in \mathbf{I}_\phi, (\phi,t,s) \in \tilde{\boldsymbol{\Omega}} \tag{17}$$

$$0 \le p^g_{\phi 1ts} \le P^G_\phi, \qquad (\phi,t,s) \in \tilde{\boldsymbol{\Omega}} \tag{18}$$

$$0 \le q^g_{\phi 1ts} \le Q^G_\phi, \qquad (\phi,t,s) \in \tilde{\boldsymbol{\Omega}} \tag{19}$$

$$p^g_{\phi its} = \sum_{h\in\mathbf{H}} \rho_{h\phi i} p^{net}_{hts} + p^w_{\phi its}, \qquad i \in \mathbf{I}_\phi \setminus \{1\}, (\phi,t,s) \in \tilde{\boldsymbol{\Omega}} \tag{20}$$

$$p^g_{\phi its} \tan\underline{\theta}_{\phi i} \le q^g_{\phi its} \le p^g_{\phi its} \tan\overline{\theta}_{\phi i}, \qquad i \in \mathbf{I}_\phi \setminus \{1\}, (\phi,t,s) \in \tilde{\boldsymbol{\Omega}} \tag{21}$$

$$-P^F_{\phi l}\lambda_{\phi lt} \le p^f_{\phi lts} \le P^F_{\phi l}\lambda_{\phi lt}, \qquad l \in \mathbf{L}_\phi, (\phi,t,s) \in \tilde{\boldsymbol{\Omega}} \tag{22}$$

$$-Q^F_{\phi l}\lambda_{\phi lt} \le q^f_{\phi lts} \le Q^F_{\phi l}\lambda_{\phi lt}, \qquad l \in \mathbf{L}_\phi, (\phi,t,s) \in \tilde{\boldsymbol{\Omega}} \tag{23}$$

$$\underline{V}^{sq}_{\phi i} \le v^{sq}_{\phi its} \le \overline{V}^{sq}_{\phi i}, \qquad i \in \mathbf{I}_\phi, (\phi,t,s) \in \tilde{\boldsymbol{\Omega}} \tag{24}$$

$$v^{sq}_{\phi its} - v^{sq}_{\phi jts} \le 2(R_{\phi l}p^f_{\phi lts} + X_{\phi l}q^f_{\phi lts})/V^{ref}_\phi + U(1-\lambda_{\phi lt}), \qquad i,j \in \mathbf{I}_\phi, l \in \mathbf{L}_\phi, (\phi,t,s) \in \tilde{\boldsymbol{\Omega}} \tag{25}$$

$$v^{sq}_{\phi its} - v^{sq}_{\phi jts} \ge 2(R_{\phi l}p^f_{\phi lts} + X_{\phi l}q^f_{\phi lts})/V^{ref}_\phi + U(\lambda_{\phi lt}-1), \qquad i,j \in \mathbf{I}_\phi, l \in \mathbf{L}_\phi, (\phi,t,s) \in \tilde{\boldsymbol{\Omega}} \tag{26}$$

$$p^{net}_{hts} = p^{h2p}_{hts} - p^{p2h}_{hts} \qquad h \in \mathbf{H}, t \in \mathbf{T}, s \in \mathbf{S} \tag{27}$$

$$E_{h(t+1)s} = E_{hts} + \left(p^{p2h}_{hts}\eta^{p2h}_h\sigma^{p2h}_h - \frac{p^{h2p}_{hts}}{\eta^{h2p}_h\sigma^{h2p}_h}\right), \qquad h \in \mathbf{H}, t \in \mathbf{T}\setminus\{|\mathbf{T}|\}, s \in \mathbf{S} \tag{28}$$

$$E_{h1s} = E^{ini}_h, \qquad h \in \mathbf{H}, s \in \mathbf{S} \tag{29}$$

$$\underline{E}_h \le E_{hts} \le \overline{E}_h, \qquad h \in \mathbf{H}, t \in \mathbf{T}, s \in \mathbf{S} \tag{30}$$

$$0 \le p^{p2h}_{hts} \le \overline{P}^{p2h}_h \mu^{p2h}_{hts}, \qquad h \in \mathbf{H}, t \in \mathbf{T}, s \in \mathbf{S} \tag{31}$$

$$0 \le p^{h2p}_{hts} \le \overline{P}^{h2p}_h \mu^{h2p}_{hts}, \qquad h \in \mathbf{H}, t \in \mathbf{T}, s \in \mathbf{S} \tag{32}$$

$$\mu^{p2h}_{hts} + \mu^{h2p}_{hts} \le 1, \qquad h \in \mathbf{H}, t \in \mathbf{T}, s \in \mathbf{S} \tag{33}$$

$$0 \le \psi_{m\phi its} \le W^{Cap}_m \beta_{m\phi it}, \qquad m \in \mathbf{M}, i \in \mathbf{I}^c_\phi, (\phi,t,s) \in \tilde{\boldsymbol{\Omega}} \tag{34}$$

$$\sum_{m\in\mathbf{M}} \psi_{m\phi its} \le \xi^w_{\phi ts}, \qquad m \in \mathbf{M}, i \in \mathbf{I}^c_\phi, (\phi,t,s) \in \tilde{\boldsymbol{\Omega}} \tag{35}$$

$$p^w_{\phi its} = \sum_{m\in\mathbf{M}} \psi_{m\phi its}, \qquad m \in \mathbf{M}, i \in \mathbf{I}^c_\phi, (\phi,t,s) \in \tilde{\boldsymbol{\Omega}} \tag{36}$$

$$p^w_{\phi its} = 0, \qquad i \in \mathbf{I}^c_\phi \setminus \mathbf{I}_\phi, (\phi,t,s) \in \tilde{\boldsymbol{\Omega}} \tag{37}$$

Constraints (14) and (15) describe the real and reactive power balance conditions at each node in each MG. The notations $\Theta(l)$ and $\Gamma(l)$ represent the source and terminal nodes of power line l, respectively.

Constraints (16) and (17) define the limits for real and reactive power outages at each node. Constraints (18) and (19) establish the lower and upper limits for real and reactive power injection at the substation node (i.e., node 1) of each MG. The real power injection at non-substation nodes is generated by the installed HSSs and connected MWTs, which is shown in constraint (20). The range of reactive power injection at non-substation nodes is set by constraint (21). The real and reactive power flows in online power lines are limited by their real and reactive capacities in constraints (22) and (23), separately. Constraints (25) and (26) represent the power flow equation considering the status of power lines where the term $U(1-\lambda_{\phi lt})$ or $U(\lambda_{\phi lt}-1)$ ensures that the power flow condition is satisfied for connected lines [44]. Constraint (24) states the boundaries for the squared voltage magnitudes at any node i of MG ϕ. Constraint (27) restricts the net real power output of HSS h. The variations in the hydrogen storage level of HSS h over time are determined by their power-to-hydrogen (P2H) and hydrogen-to-power (H2P) operation modes, as denoted in constraint (28). Constraint (29) defines the initial hydrogen storage level setting of HSS h. Constraint (30) specifies the range of the hydrogen storage level of HSS h. Constraints (31) and (32) impose the limits for P2H and H2P outputs of HSS h, respectively. Constraint (33) indicates that P2H and H2P modes of HSS h are mutually exclusive. Constraint (34) guarantees that the power output of MWT m does not exceed its capacity if it is connected. The total power output of MWTs cannot be greater than the predicted wind energy in MG ϕ at time t, which is denoted by constraint (35). Constraints (36) and (37) stipulate the total power injection from all possible MWTs to each node of each MG.

5. Numerical results and discussions

5.1. Test system characteristics and assumptions

In this section, the effectiveness of the proposed service restoration model is verified by application to a test case that integrates a TS and multiple MGs — a central Alabama interstate transportation network [45] (see Fig. 6), and four IEEE 33-node distribution systems [44]. The configuration of the test system is illustrated in Fig. 7, where MGs and TS networks are integrated through several coupling nodes. Detailed information on HSSs can be found in [46]. Six MWTs are considered in the test system, each with 50 kW capacity [47]. Given the information of the TS, the traveling time $T^{r}_{k\hat{k}}$ can be obtained through the shortest-path algorithm described in Section 3.2. We initially generate 500 wind forecast scenarios based on the Weibull distribution using the Monte Carlo simulation. We then employ the Backward Scenario Reduction algorithm to obtain a final set of 20 wind forecast scenarios (see Section 3.3). The entire restoration time horizon in all conducted tests is assumed to be 24 periods of 30-minute duration (i.e. 12 h). We investigate the impact of the joint operation of MWTs and HSSs on power system resilience by studying three different cases on the test system:

- **Case I**: Three-Line Damage Scenario in each MG.
- **Case II**: Five-Line Damage Scenario in each MG.
- **Case III**: Eight-Line Damage Scenario in each MG.

Numerical tests are conducted on a machine with an Intel i7-8700 processor and 32 GB RAM. The optimization problem is formulated with AMPL and solved with the state-of-the-art optimization solver Gurobi 10.0.0.

5.2. Spatiotemporal travel dynamics of MWTs

The detailed routing and scheduling decisions on MWTs 1–6 in each studied case are exhibited in Fig. 8, and analyzed as follows.

Case I: MWT1 and MWT2 start at depot (i.e., TS node 14) and are then scheduled to visit TS node 12 between t_2 - t_4, followed by TS node 13 from t_9 - t_{10}. MWT3 and MWT4 also start at the same depot and are then scheduled to visit TS node 5 between t_2 - t_6. Afterwards, MWT3 is scheduled to travel to TS node 2 from t_{12} - t_{13} and then to TS node 1 from t_{19} - t_{20}, while MWT4 is scheduled to travel to TS node 4 from t_{10} - t_{11}, and then to TS node 2 from t_{14} - t_{15}. MWT5 starts at the depot and is scheduled to visit TS node 17 between t_2 -t_5, followed by TS node 21 from t_7 - t_9, and then TS node 23 from t_{13} - t_{16}. MWT6 starts at the depot and is scheduled to visit TS node 20 between t_2 - t_5, followed by TS node 23 from t_{14} - t_{15}.

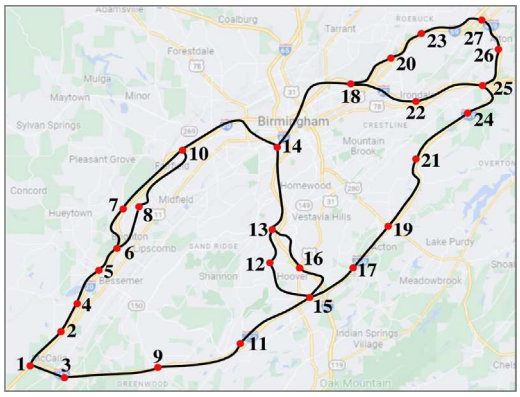

Fig. 6. The central Alabama interstate transportation network [45].

Case II: MWT1 is assigned to visit TS node 5 between t_2 - t_6 and TS node 2 from t_9 - t_{10}. MWT2 is assigned to visit TS node 17 between t_2 - t_5 and TS node 21 from t_{13} - t_{15}. MWT3 is assigned to visit TS node 2 between t_2 - t_7, TS node 4 from t_{13} - t_{14}, and then TS node 2 from t_{19} - t_{20}. MWT4 is assigned to visit TS node 12 between t_2 - t_4, TS node 16 from t_{15} - t_{16}, and then TS node 21 from t_{18} - t_{21}. MWT5 and MWT6 are both assigned to visit TS node 10 between t_2 - t_4 and TS node 7 from t_{13} to t_{14}.

Case III: MWT1 travels from depot to TS node 2 between t_2 -t_7. MWT2 moves from its depot to TS node 17 between t_2 - t_5, and is then sent to TS node 21 from t_{13} - t_{15}. MWT3 travels from its depot to TS node 5 between t_2 - t_6. MWT4 moves from its depot to TS node 4 between t_2 - t_6, and is then sent to TS node 2 from t_8 - t_9. MWT5 travels from its depot to TS node 20 between t_2 - t_5, and is then sent to TS node 23 from t_{13} - t_{14}. MWT6 moves from its depot to TS node 5 between t_2 - T_5, and is then sent to TS node 2 from t_{17} - t_{19}.

5.3. Analysis of MWTs contribution to service restoration

The results presented in Fig. 9 illustrate the percentage of restored demand across multiple MGs under different studied cases (i.e., damage scenarios). As shown in the figure, the use of MWTs results in a significantly higher percentage of restored demand compared to the scenarios without MWTs. This indicates that incorporating MWTs into the restoration process can facilitate faster and more efficient recovery of power. Specifically, as depicted in Figs. 9(a) and 9(b), the utilization of MWTs enables the complete restoration of the total power outage one hour earlier than the case in the absence of MWTs. Table 1 indicates that incorporating MWTs can lead to a reduction of approximately 16% ($31,834k vs. $37,898k) in total costs of power outages for **Case I**, 16.29% ($32,571k vs. $38,908k) for **Case II**, and 12.66% ($39,537k vs. $45,268k) for **Case III**. The results presented in both Fig. 9 and Table 1 demonstrate that incorporating MWTs can have a substantial positive impact on improving the resilience of rural communities and critical infrastructures during HILP events.

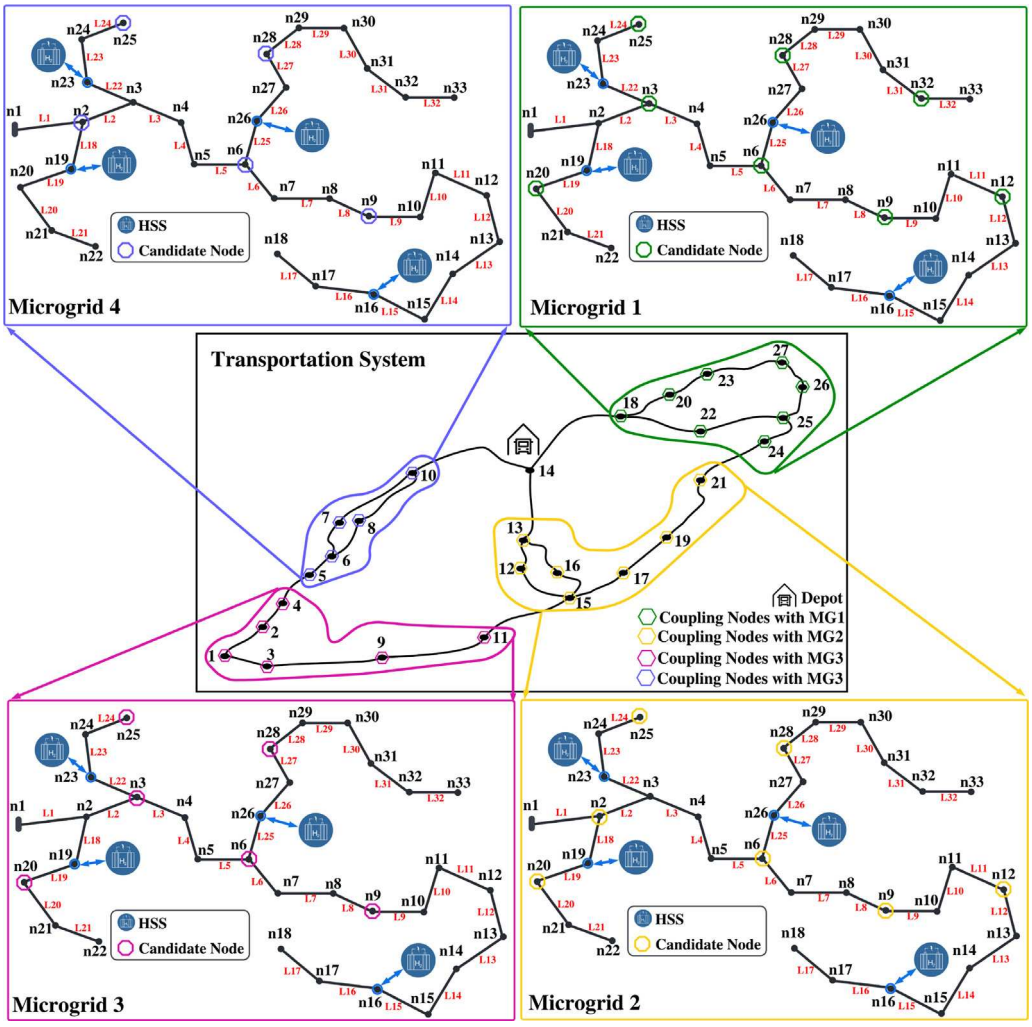

Fig. 7. An integrated test system with a central Alabama interstate transportation network and four MGs.

Table 1
Total costs of power outages with and without MWTs.

	Case I	Case II	Case III
With MWTs ($)	31,834k	32,571k	39,537k
Without MWTs ($)	37,898k	38,908k	45,268k
Saving (%)	16	16.29	12.66

5.4. Impact analysis of the number of available MWTs

In this subsection, we assess the effectiveness of the proposed model by examining the capacity utilization rate (CUR) of MWTs throughout the restoration process and the corresponding power outage costs for varying numbers of MWTs. This evaluation allows us to determine the optimal number of MWTs to use in order to achieve the best balance between resource utilization and cost efficiency. In this study, the CUR of MWTs is defined as follows:

$$CUR = \frac{\sum_{s\in\mathbf{S}} \pi_s \sum_{\phi\in\boldsymbol{\Phi}} \sum_{i\in\mathbf{I}_\phi} \sum_{t\in\mathbf{T}} p^{w}_{\phi,i,t,s}}{|\mathbf{T}| \sum_{m\in\mathbf{M}} W^{Cap}_{m}}$$

Fig. 10 presents a comprehensive analysis of the expected power outage costs, MWTs' investment costs, total costs, and CUR values for four MWTs under various scenarios. The quantity of MWTs considered in this analysis is 6, 10, 12, and 15. The results provide valuable insights into the relationship between the number of MWTs utilized and the associated costs and CUR. Fig. 10 demonstrates that the value of CUR decreases significantly from 6 MWTs to 10 MWTs, with reductions from 72% to 55% in **Case I**, 62% to 50% in **Case II**, and 63% to 53% in **Case III**. However, when the number of MWTs increases from 10 to 15, the CUR decreases at a slower pace. Additionally, it is observed that an increase in the number of MWTs corresponds to a decrease in the expected power outage costs, albeit at the cost of higher MWTs investments. Total costs, defined as the sum of the expected power outage costs and the MWTs' investment costs, are therefore influenced by the balance between these two factors. Based on a cost–benefit analysis, it is evident that utilizing 15 MWTs is not the most cost-effective option when considering the total costs. In **Case I**, the optimal solution is found to be 12 MWTs, with a cost of $35M. In **Case II** and **Case III**, the cheapest option is 10 MWTs, with total costs of $35.89M and $42.58M, respectively. Therefore, the choice of the optimal number of MWTs depends on the specific priorities and constraints of the restoration process. If priority is given to achieving higher values of CUR, then 6 MWTs are recommended. On the other hand, if minimizing the expected power outage costs is the primary objective, 15 MWTs would be the preferred option. However, if a balance between these two factors is sought, then 10 MWTs emerge as the most cost-effective solution.

5.5. Impact analysis of collected information to service restoration

In this subsection, we conduct a sensitivity analysis on various types of collected information, as depicted in Fig. 5. This includes analyses

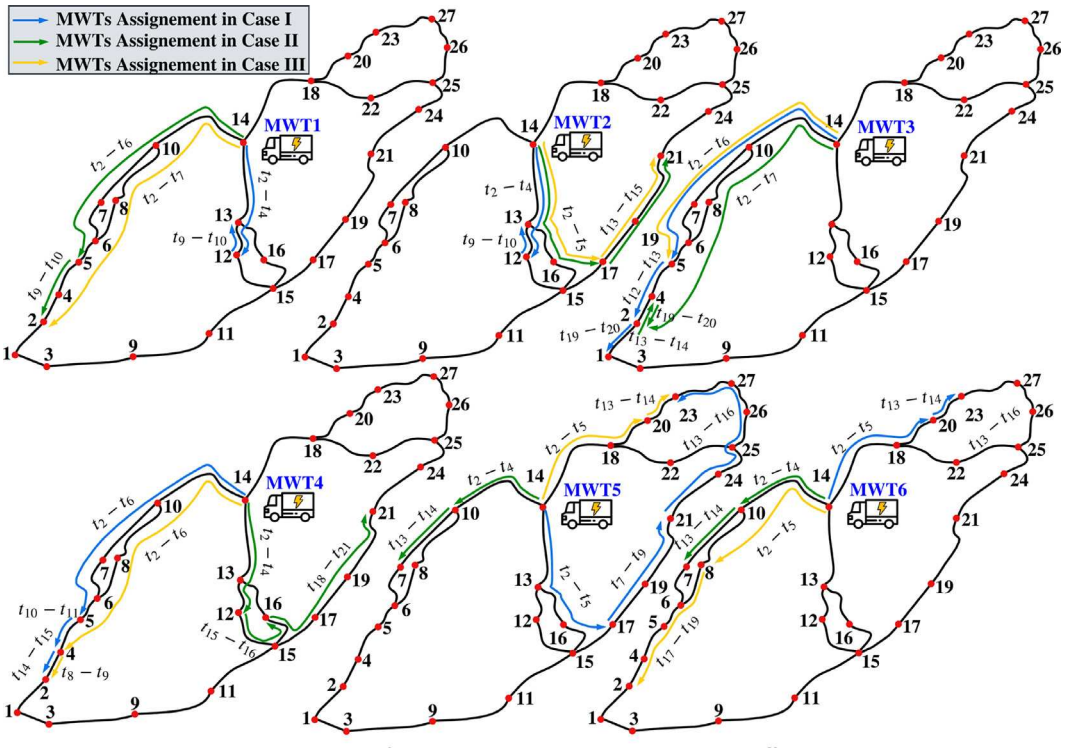

Fig. 8. MWTs assignments for response and recovery in different damage scenarios.

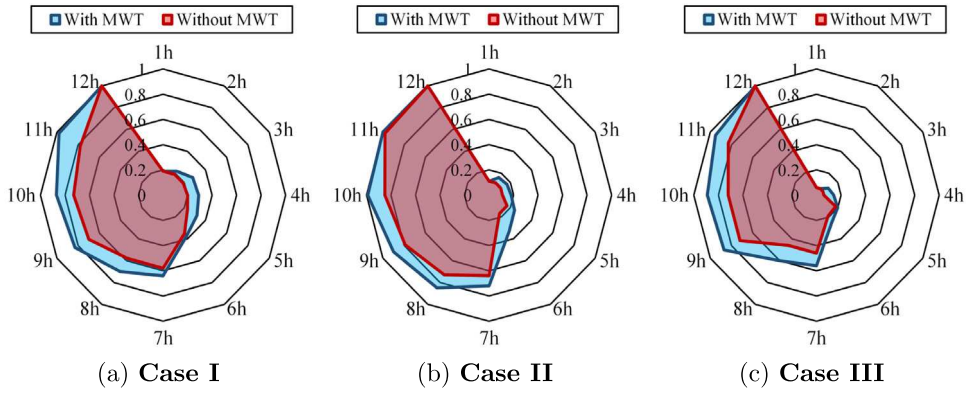

Fig. 9. Percentage of total restored demand over time under different cases.

of travel time information, line failure information, and wind power prediction.

Firstly, to assess the role of MWTs in reducing power outage costs, regardless of line failure specifics, we generate 100 random line failure scenarios in each MG using Monte Carlo Simulation. Each scenario is independently analyzed using the proposed two-stage optimization model to evaluate the performance. These results are summarized in Table 2, showing the maximum, minimum, mean, and standard deviation values of the total costs associated with power outages. Comparing the results in Table 2 with Table 1, the reductions in power outage costs for the considered study cases align well within the range of the 100 scenarios. For instance, the cost reduction percentages in **Case I** and **Case II** are around 16%, close to the mean value reported in Table 2 (17.42%). The reduction percentage in **Case III** exceeds the minimum value in Table 2 (12.66% vs. 10.49%).

Secondly, in evaluating the effectiveness of MWTs in lowering power outage costs under various levels of wind power availability, we adjust the location parameter of the Weibull distribution. This adjustment creates scenarios representing both insufficient and sufficient wind power availability. For each of these scenarios, we implement the proposed model under the three study cases previously described. Table 3 provides insights into this relationship. It shows that the availability of sufficient wind power in the surrounding environment significantly enhances the contribution of MWTs in reducing power outage costs. This finding highlights the critical role of wind power availability in maximizing the cost-saving potential of MWTs. As wind power availability increases, MWTs become more effective in mitigating power outage expenses, underlining the importance of considering

Table 2
Power outage costs reported by the proposed model with 100 randomly-generated failure scenarios.

	Max.	Min.	Mean	Standard deviation
With MWTs ($)	54,294k	17,916k	33,623k	8095k
Without MWTs ($)	60,659k	22,707k	40,696k	9499k
Saving (%)	22.95	10.49	17.42	2.47

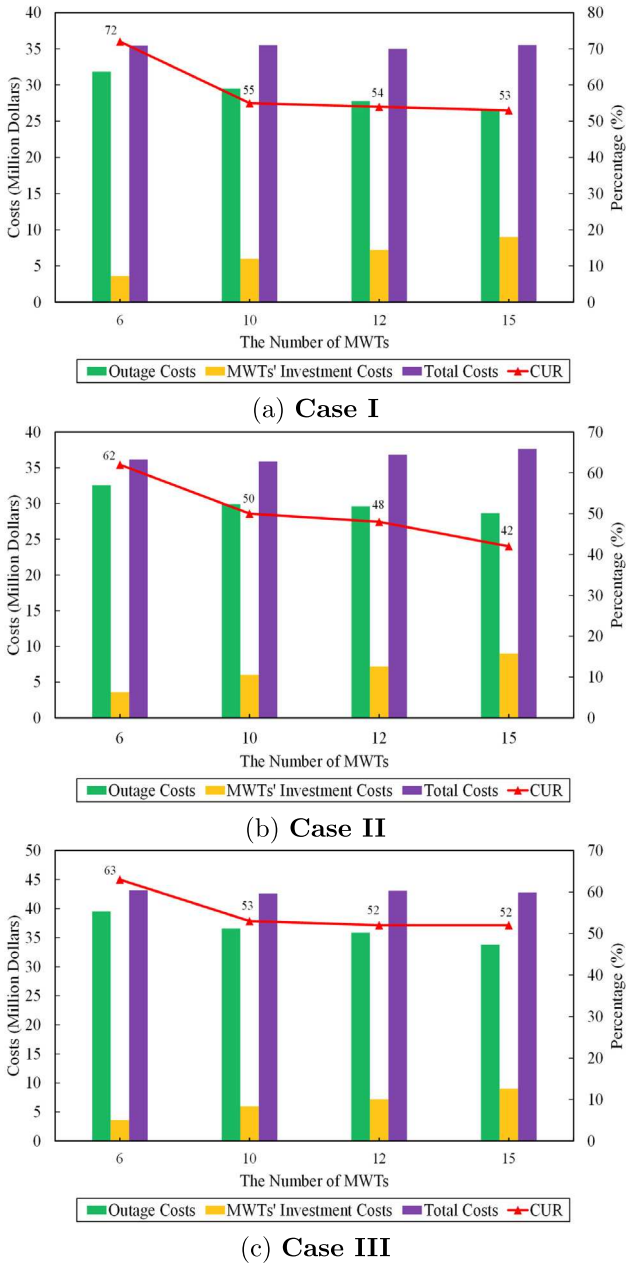

Fig. 10. Costs and CUR under variable availability of MWT units.

Table 3
Total costs of power outages under different levels of wind power availability.

Wind power		With MWTs ($)	Without MWTs ($)	Saving (%)
Insufficient	Case I	33,527k	37,898k	11.53
	Case II	34,171k	38,908k	12.17
	Case III	40,116k	45,268k	11.38
Sufficient	Case I	31.385k	37,898k	17.18
	Case II	32,580k	38,908k	16.26
	Case III	39,199k	45,268k	13.41

environmental wind conditions in the strategic deployment of MWTs for power restoration.

Lastly, to evaluate the impact of MWTs on reducing power outage costs in relation to travel time information, we account for two distinct levels of damage severity in the TS — low and high. Using the shortest-path algorithm, we calculate the travel times corresponding to each

Table 4
Total costs of power outages under different levels of damage severity in the TS.

Severity level		With MWTs ($)	Without MWTs ($)	Saving (%)
Low	Case I	31,898k	37,898k	16.61
	Case II	32,597k	38,908k	16.22
	Case III	38,673k	45,268k	14.57
High	Case I	33,287k	37,898k	12.17
	Case II	33,954k	38,908k	12.73
	Case III	41,794k	45,268k	7.67

severity level. Subsequently, the proposed model is executed for each travel time scenario within our designated three study cases. Table 4 details the total power outage costs under varying damage severity levels in the TS. An analysis of Table 4 reveals that the reduction in outage costs is less pronounced in scenarios with a higher level of damage severity compared to those with a lower level. This indicates that lower severe damage in the TS can improve the effectiveness of MWTs in reducing outage costs, emphasizing the importance of TS conditions in the overall efficiency of the proposed restoration strategy. This insight underscores the interdependency between TS integrity and the effectiveness of MWT deployment in emergency power restoration scenarios.

5.6. Analysis of MWTs contribution to decarbonization

In this subsection, we assess the role and contributions of MWTs to decarbonization targets, by comparing it to the conventional approach of using mobile emergency generators (MEGs) for service restoration. Specifically, we investigate the performance of different numbers of MEGs, under the same settings as in all studied cases earlier. We estimate the carbon dioxide (CO_2) emissions resulting from the use of MEGs during the restoration process based on the report by the U.S. Environmental Protection Agency [48]. This evaluation allows us to compare the environmental impacts of using MWTs versus MEGs in the power restoration processes.

Table 5 presents a comparison of the CO_2 emissions and power outage costs resulting from the utilization of different numbers of MWTs and MEGs. Our analysis reveals that, when compared to MWTs, MEGs can lead to lower power outage costs but higher CO_2 emissions. Across all studied cases, we observe that the use of 10 MEGs can reduce power outage costs more significantly than MWTs, with a reduction of nearly 8.7%. On the other hand, with 6 MWTs, power outage costs are similar for both MWTs and MEGs. However, it is important to note that the use of more MEGs results in higher CO_2 emissions. Therefore, our analysis indicates that the utilization of MWTs represents a more environmentally friendly approach to service restoration compared to MEGs. This is particularly true when a limited number of MWTs are used, as it enables the achievement of zero CO_2 emissions while keeping power outage costs as low as possible. These findings demonstrate the potential of MWTs in promoting sustainable power restoration processes, which are crucial in mitigating the negative impact of power outages on both the environment and society.

6. Conclusion

This paper proposed a novel service restoration scheme to enhance the resilience of hydrogen-accommodated MGs through optimal decisions on the routing and scheduling of MWTs. The proposed approach employs the shortest-path algorithm to obtain the traveling time required for MWTs to reach the desired location along the TS, facilitating the development of a more efficient and sustainable power restoration process. The proposed problem takes the form of a two-stage stochastic optimization model and captures the uncertainty of wind power prediction, which is captured by generating scenarios using Monte

Table 5
Performance comparison of MWTs and MEGs.

Technology	Test case	Available units	Outage costs ($)	CO_2 emission (ton)
MWT	I	6	31,834k	0
		10	29,509k	0
	II	6	32,571k	0
		10	30,897k	0
	III	6	39,537k	0
		10	36,578k	0
MEG	I	6	31,648k	7.27
		10	26,549k	12.19
	II	6	32,267k	7.62
		10	28,467k	13.48
	III	6	38,701k	8.28
		10	33,476k	14.75

Carlo simulation following a Weibull distribution. Numerical results on an integrated transportation and energy network – a central Alabama interstate transportation network and four IEEE 33-node distribution systems – highlighted the benefit and efficacy of the proposed approach in boosting MGs resilience against HILP extremes while achieving decarbonization targets. The analyses of the results provided insights into the optimal selection of the number of MWTs, considering trade-offs among the expected power outage costs, CUR values, and CO_2 emission.

CRediT authorship contribution statement

Jinshun Su: Conceptualization, Data curation, Formal analysis, Investigation, Methodology, Software, Validation, Visualization, Writing – original draft, Writing – review & editing. **Ruotan Zhang:** Data curation, Formal analysis, Visualization, Writing – original draft, Writing – review & editing. **Payman Dehghanian:** Conceptualization, Funding acquisition, Investigation, Project administration, Resources, Software, Supervision, Validation, Writing – original draft, Writing – review & editing. **Mohammad Heidari Kapourchali:** Investigation, Writing – original draft, Writing – review & editing. **Sungyun Choi:** Investigation, Writing – original draft, Writing – review & editing. **Zhaohao Ding:** Investigation, Writing – original draft, Writing – review & editing.

Declaration of competing interest

The authors declare that they have no known competing financial interests or personal relationships that could have appeared to influence the work reported in this paper.

Data availability

Data will be made available on request.

Acknowledgment

This work was supported in part by the National Science Foundation (NSF) under Grants ECCS-2114100, RISE-2220626, RISE-2220624, and OIA-2229772.

References

[1] Anokhin D, Dehghanian P, Lejeune MA, Su J. Mobility-as-a-service for resilience delivery in power distribution systems. Prod Oper Manage 2021;30(8):2492–521.
[2] NCEI. Billion-dollar weather and climate disasters. 2022, Available at https://www.ncei.noaa.gov/access/billions/references. [Accessed 2022].
[3] Dehghanian P, Zhang B, Dokic T, Kezunovic M. Predictive risk analytics for weather-resilient operation of electric power systems. IEEE Trans Sustain Energy 2019;10(1):3–15.
[4] Kossin JP, Emanuel KA, Vecchi GA. The poleward migration of the location of tropical cyclone maximum intensity. Nature 2014;509(7500):349–52.
[5] Mitigation Assessment Team. Hurricanes Irma and Maria in puerto rico: building performance observations, recommendations, and technical guidance. FEMA; 2018.
[6] Comes T, Van de Walle BA. Measuring disaster resilience: The impact of hurricane sandy on critical infrastructure systems. ISCRAM 2014;11(May):195–204.
[7] Abatzoglou JT, Williams AP. Impact of anthropogenic climate change on wildfire across western US forests. Proc Natl Acad Sci 2016;113(42):11770–5.
[8] Jones D. October wildfire claims top $9.4 billion statewide. California Department of Insurance; 2017, http://www.insurance.ca.gov/0400-news/0100-press-releases/2017/release135-17.cfm.
[9] Hoover K, Hanson LA. Wildfire statistics. Tech. rep., Congressional Research Service; 2021.
[10] Hartmann DL. Pacific sea surface temperature and the winter of 2014. Geophys Res Lett 2015;42(6):1894–902.
[11] Busby JW, Baker K, Bazilian MD, Gilbert AQ, Grubert E, Rai V, Rhodes JD, Shidore S, Smith CA, Webber ME. Cascading risks: Understanding the 2021 winter blackout in Texas. Energy Res Soc Sci 2021;77:102106.
[12] Yan J. The impact of climate policy on fossil fuel consumption: Evidence from the regional greenhouse gas initiative (RGGI). Energy Econ 2021;100:105333.
[13] Wang S, Dehghanian P, Alhazmi M, Su J, Shinde B. Resilience-assured protective control of DC/AC inverters under unbalanced and fault scenarios. In: 2019 IEEE power & energy society innovative smart grid technologies conference. ISGT, 2019, p. 1–5.
[14] Huo X, Dong J, Cui B, Liu B, Lian J, Liu M. Two-level decentralized-centralized control of distributed energy resources in grid-interactive efficient buildings. IEEE Control Syst Lett 2023;7:997–1002.
[15] Qiu F, Zhang Y, Yao R, Du P. Power system restoration with renewable participation. IEEE Trans Sustain Energy 2023;14(2):1112–21.
[16] Su J, Dehghanian P, Nazemi M, Wang B. Distributed wind power resources for enhanced power grid resilience. In: 2019 North American power symposium. NAPS, 2019, p. 1–6.
[17] Choopani K, Effatnejad R, Hedayati M. Coordination of energy storage and wind power plant considering energy and reserve market for a resilience smart grid. J Energy Storage 2020;30:101542.
[18] Golshani A, Sun W, Zhou Q, Zheng QP, Wang J, Qiu F. Coordination of wind farm and pumped-storage hydro for a self-healing power grid. IEEE Trans Sustain Energy 2018;9(4):1910–20.
[19] Li S, Wang L, Gu X, Zhao H, Sun Y. Optimization of loop-network reconfiguration strategies to eliminate transmission line overloads in power system restoration process with wind power integration. Int J Electr Power Energy Syst 2022;134:107351.
[20] Sun L, Liu W, Chung C, Ding M, Ding J. Rolling optimization of transmission network recovery and load restoration considering hybrid wind-storage system and cold load pickup. Int J Electr Power Energy Syst 2022;141:108168.
[21] Liu W, Liu Y, Wu L. Model predictive control based voltage regulation strategy using wind farm as black-start source. IEEE Trans Sustain Energy 2023;14(2):1122–34.
[22] Yao S, Wang P, Zhao T. Transportable energy storage for more resilient distribution systems with multiple microgrids. IEEE Trans Smart Grid 2018;10(3):3331–41.
[23] Yao S, Wang P, Liu X, Zhang H, Zhao T. Rolling optimization of mobile energy storage fleets for resilient service restoration. IEEE Trans Smart Grid 2019;11(2):1030–43.
[24] Saboori H, Mehrjerdi H, Jadid S. Mobile battery storage modeling and normal-emergency operation in coupled distribution-transportation networks. IEEE Trans Sustain Energy 2022;13(4):2226–38.
[25] Lei S, Chen C, Li Y, Hou Y. Resilient disaster recovery logistics of distribution systems: Co-optimize service restoration with repair crew and mobile power source dispatch. IEEE Trans Smart Grid 2019;10(6):6187–202.
[26] Ding T, Wang Z, Jia W, Chen B, Chen C, Shahidehpour M. Multiperiod distribution system restoration with routing repair crews, mobile electric vehicles, and soft-open-point networked microgrids. IEEE Trans Smart Grid 2020;11(6):4795–808.
[27] Yang Z, Dehghanian P, Nazemi M. Seismic-resilient electric power distribution systems: Harnessing the mobility of power sources. IEEE Trans Ind Appl 2020;56(3):2304–13.
[28] Wu H, Xie Y, Wu Q, Yu C, Sun J. A three-stage resilient dispatch of mobile emergency generators in a distribution system against hurricanes. Int J Electr Power Energy Syst 2023;148:108844.
[29] Nazemi M, Dehghanian P, Lu X, Chen C. Uncertainty-aware deployment of mobile energy storage systems for distribution grid resilience. IEEE Trans Smart Grid 2021;12(4):3200–14.
[30] Su J, Anokhin D, Dehghanian P, Lejeune MA. On the use of mobile power sources in distribution networks under endogenous uncertainty. IEEE Trans Control Netw Syst 2023;10(4):1937–49.
[31] Su J, Mehrani S, Dehghanian P, Lejeune MA. Quasi second-order stochastic dominance model for balancing wildfire risks and power outages due to proactive public safety de-energizations. IEEE Trans Power Syst 2024;39(2):1–14.

[32] Erdemir G, Kuzucuoğlu AE, Selçuk FA. A mobile wind turbine design for emergencies in rural areas. Renew Energy 2020;166:9–19.
[33] Uprise Energy. Portability. 2023, [Online] Available at: https://upriseenergy.com/portability.
[34] Song D, Liu J, Yang J, Su M, Wang Y, Yang X, Huang L, Joo YH. Optimal design of wind turbines on high-altitude sites based on improved Yin–Yang pair optimization. Energy 2020;193:116794.
[35] Su J, Dehghanian P, Vergara B, Kapourchali MH. An energy management system for joint operation of small-scale wind turbines and electric thermal storage in isolated microgrids. In: 2021 North American power symposium. NAPS, 2021, p. 1–6.
[36] El-Taweel NA, Khani H, Farag HE. Hydrogen storage optimal scheduling for fuel supply and capacity-based demand response program under dynamic hydrogen pricing. IEEE Trans Smart Grid 2018;10(4):4531–42.
[37] Shams MH, Mansour-Lakouraj M, Liu JJ, Javadi MS, Catalão JP. Learning-based coordinated operation of multiple microgrids with hydrogen systems: A novel bilevel framework. IEEE Ind Appl Mag 2022;29(2):45–58.
[38] Magzhan K, Jani HM. A review and evaluations of shortest path algorithms. Int J Sci Technol Res 2013;2(6):99–104.
[39] Sudhakar T, Vadivoo NS, Slochanal SMR, Ravichandran S. Supply restoration in distribution networks using Dijkstra's algorithm. In: 2004 international conference on power system technology, 2004. PowerCon 2004. Vol. 1, IEEE; 2004, p. 640–5.
[40] Dehghanian P, Kezunovic M. Probabilistic decision making for the bulk power system optimal topology control. IEEE Trans Smart Grid 2016;7(4):2071–81.
[41] Li W. Risk assessment of power systems: models, methods, and applications. John Wiley & Sons; 2014.
[42] Trakas DN, Hatziargyriou ND. Optimal distribution system operation for enhancing resilience against wildfires. IEEE Trans Power Syst 2017;33(2):2260–71.
[43] Heitsch H, Römisch W. Scenario reduction algorithms in stochastic programming. Comput Optim Appl 2003;24:187–206.
[44] Baran ME, Wu FF. Network reconfiguration in distribution systems for loss reduction and load balancing. IEEE Power Eng Rev 1989;9(4):101–2.
[45] Nie Q, Qian X, Guo S, Jones S, Doustmohammadi M, Anderson MD. Impact of COVID-19 on paratransit operators and riders: A case study of central Alabama. Transp Res A 2022;161:48–67.
[46] Dong Y, Zheng W, Cao X, Sun X, He Z. Co-planning of hydrogen-based microgrids and fuel-cell bus operation centers under low-carbon and resilience considerations. Appl Energy 2023;336:120849.
[47] Uprise Energy. 50kW portable power center. 2023, [Online] Available at: https://upriseenergy.com/50kw-portable-power-center.
[48] US Environmental Protection Agency. Emission factors for greenhouse gas inventories. 2018, https://www.epa.gov/sites/default/files/2018-03/documents/emission-factors_mar_2018_0.pdf.